THE ASTROPHYSICAL JOURNAL, 262:478–496, 1982 November 15

RELATIVISTIC PRECESSING JETS IN QUASARS AND RADIO GALAXIES: MODELS TO FIT HIGH RESOLUTION DATA

ANN C. GOWER
Department of Physics, University of Victoria
P. C. GREGORY
Department of Physics, University of British Columbia
J. B. HUTCHINGS
Dominion Astrophysical Observatory, Herzberg Institute of Astrophysics
AND
W. G. UNRUH
Department of Physics, University of British Columbia
Received 1982 January 12; accepted 1982 April 26

ABSTRACT

We present the formulation of generalized models tracing the geometry and intensity of the synchrotron emission from precessing, twin, relativistic jets as projected on the plane of the sky. We show that neither the shape of the image nor its relative intensities are altered by including the effects of a cosmological redshift and a relative velocity between the source and observer. The models are fitted to the available data for several quasars and radio galaxies and demonstrate the plausibility of the phenomenon. Probable selection effects are considered and diagnostics given for recognizing objects showing this behavior. In the radio galaxies considered, velocities up to $\sim 0.2c$ and precession periods of $\sim 10^6$ yr are deduced. In the QSOs investigated, velocities of $0.7c$ and greater are found and periods of order 10^4 yr. In some cases precession cone angles increase with time. Consequences in terms of lifetimes of QSO behavior and binary supermassive objects are discussed.

Subject headings: quasars — radio sources: galaxies

I. INTRODUCTION

Recent high-resolution radio maps of quasars have shown up a class of objects with complex structure on the scale of seconds of arc, often asymmetric (e.g., Perley, Fomalont, and Johnston 1980; Ulvestad *et al.* 1981; Neff 1982), which is unlike the classic double radio source or the straight "jet." Some of these have been described as "curved" or "bent" jets, while others are of more complex morphology. Some radio galaxies also show complex curved structure, such as the Z-shaped sources NGC 326 or 3C 315. In recent studies, cases have been made for regular precession in some of these objects (e.g., NGC 326 Ekers *et al.* 1978; 3C 129 Icke 1981; 4C 18.68 Gower and Hutchings 1982), and much credibility has been added to the general idea of jet precession by the direct observation of the phenomenon in the extraordinary galactic object SS 433 (Hjellming and Johnston 1981).

It has been suggested (Scheuer and Readhead 1979; Blandford and Königl 1979) that quasars may be radio sources whose emission is in a relativistic jet beamed towards the observer so that we see the emission greatly enhanced in intensity by the Doppler effect. If we suppose that at least some of these objects are undergoing a nuclear event which leads to rotation or precession of the central jet-emitting object, then the relativistic jets will describe curved paths. In this paper we explore the possibility that the observed arc-second radio structure of some quasars represents the path traced out by material flung out, still at relativistic speed, by the precessing beam and now moving radially outwards. Some models of this nature have been discussed by Linfield (1981). In his study, the main interest was in the propagation of inhomogeneities in the innermost part of the curved jet.

We first present the formulation we have used for modeling relativistic and nonrelativistic precessing jets and their projection on the sky. Some grids of models and general diagnostics for recognizing and fitting such models are then discussed. We then show that a very good fit can be made to the radio data for several quasars and radio galaxies. Finally we discuss the plausibility of the phenomenon in active galactic nuclei and the implied consequences in understanding the QSO phenomenon.

II. THEORY

In this section we introduce the model and discuss the equations used to describe the appearance of the precessing twin-jet model as projected on to the sky plane; i.e., a "snapshot" of the jets at some observed epoch. The initial stages of this treatment are similar to that given by Hjellming and Johnston (1981) in their analysis of the proper motions of SS 433 which concentrated on the observed structure of the jets under the conditions of no relative velocity between the observer and the source, and a flat spacetime. This of course neglects any possible effect of the source redshift on the jet image which could be important when dealing with quasar images. Our treatment also includes a discussion of the relative intensities within the image. We will show that in fact neither a cosmological redshift nor a relative velocity between observer and source alters the conclusions obtained from the assumptions of flat spacetime and no relative velocity.

a) Kinematic Model

We start with a discussion of the equations appropriate for flat spacetime and no relative velocity of source and observer. For the purpose of this analysis, it is convenient to treat each jet as a stream of identical packets of radiating matter (plasmons), but we do not mean to imply by this that the jets are discrete rather than continuous. The plasmons are ejected at a fixed speed $\beta = v/c$ with respect to the source, in two opposite directions, and the velocity vector of any individual plasmon remains constant in time. The source is at rest at the origin of the right-handed coordinate system, x', y', z' as shown in Figure 1. The y' axis is in the sky plane, and z' is the axis about which the plasmon ejection velocity precesses with an angular velocity Ω and at an angle ψ. Consider a second right-handed coordinate system x, y, z which is formed by rotating the x', y', z' axes about the y' axis until the z axis is in the sky plane and the x axis coincides with the line of sight to the observer located at a distance d from the source. The precession axis z' lies in the x-z plane and is inclined to the line of sight by the angle i.

Let t represent the time recorded by a clock at rest in the x, y, z frame, which is adjacent to any particular event in spacetime. Let ${}_0t$ be the corresponding time recorded by a clock at the location of the observer which differs from t by the light travel time from the event to the observer. If we consider two events along the path of a particular plasmon, then Δt and $\Delta_0 t$ are related by

$$\Delta t = \Delta_0 t/(1 - v_x/c),$$

where v_x is the component of the velocity along the line of sight. Also

$$\Delta t = \Delta\tau/(1 - v^2/c^2)^{1/2},$$

where $\Delta\tau$ is the proper time interval in the reference frame of the plasmon.

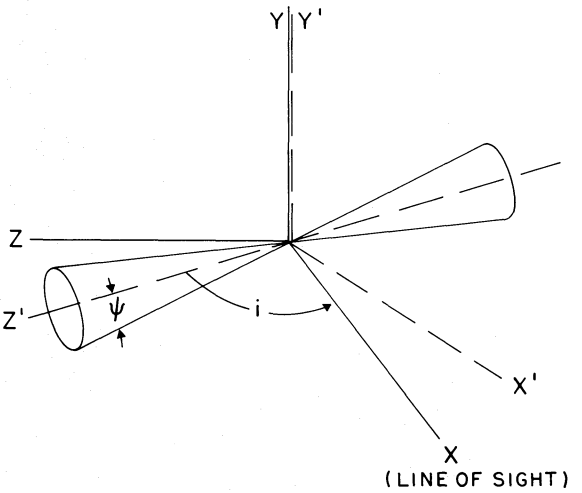

FIG. 1.—The two coordinate systems used in deriving the models. Z is jet precession axis and ψ the cone angle. X is the line of sight, and YZ the plane of the sky.

The ejection velocity vector $\boldsymbol{v}$ can be specified in terms of spherical polar coordinates with ψ as the polar angle and $\Omega(t_{ej}-t_{ref})$ the azimuthal angle, for some ejection time t_{ej} after a reference time t_{ref} when the velocity vector lies in the x-z plane. Following Hjellming and Johnston (1981) we can write for the velocity components of a plasmon along the x, y, z axes,

$$v_x = s_{jet}\beta c\left[\sin\psi \sin i \cos\Omega(t_{ej}-t_{ref})+\cos\psi\cos i\right], \tag{1}$$

$$v_y = s_{jet}\beta c \sin\psi \sin\Omega(t_{ej}-t_{ref}), \tag{2}$$

and

$$v_z = s_{jet}\beta c\left[\cos\psi \sin i - \sin\psi\cos i\cos\Omega(t_{ej}-t_{ref})\right], \tag{3}$$

where s_{jet} is a sign parameter equal to $+1$ for the jet moving mostly towards the observer and equal to -1 for the counterjet.

At some later time t_1, the coordinates of the plasmon on the sky plane are $z = v_z(t_1 - t_{ej})$ and $y = v_y(t_1 - t_{ej})$. In terms of the time interval recorded by the observer's clock, the angular motion of the jet is given by

$$\phi_z = v_z({}_0t_1 - {}_0t_{ej})/[d(1-v_x/c)] \tag{4}$$

and

$$\phi_y = v_y({}_0t_1 - {}_0t_{ej})/[d(1-v_x/c)]. \tag{5}$$

Equations (1)–(5) can thus be used to provide a "snapshot" of the shape of the precessing jets at some particular epoch ${}_0t_1$. This is achieved by fixing ${}_0t_1$ and varying ${}_0t_{ej}$ from ${}_0t_1$ to 0. It is convenient to express the azimuthal angle as a function of $({}_0t_1 - {}_0t_{ej})$ as well:

$$\Omega(t_{ej}-t_{ref}) = \Omega\left[({}_st_1 - t_{ref}) - ({}_st_1 - t_{ej})\right],$$

where ${}_st_1$ is the time that would be recorded for an event located at the source which would be observed at the telescope at the time ${}_0t_1$. Since the events represented by ${}_st_1$ and t_{ej} occur at the same location, i.e., the source, then $({}_st_1 - t_{ej}) = ({}_0t_1 - {}_0t_{ej})$. Also, since both ${}_st_1$ and t_{ref} are constants, we can set $\Omega({}_st_1 - t_{ref}) = \theta$ where θ corresponds to the azimuth of ejection for the plasmon which was being ejected at the time of the "snapshot," ${}_0t_{ej} = {}_0t_1$.

Therefore,

$$\Omega(t_{ej}-t_{ref}) = \theta - \Omega({}_0t_1 - {}_0t_{ej}). \tag{6}$$

In constructing images we have found it convenient to compute values of ϕ_y, ϕ_z as a function of a scaling parameter r given by

$$r = \beta c \cos\psi \sin i({}_0t_1 - {}_0t_{ej})/d. \tag{7}$$

For models in which $\psi \leq i$, this leads to an image size $\sim 2\, r_{max}$ in whatever units are desired, regardless of the particular choice of model parameters.

The principal effect of β on the geometry of these models arises from the light travel time factor, $[1-(v_x/c)]^{-1}$, which causes a stretching of the approaching jet and compression of the receding jet because of a change in sign of v_x for the two jets. Figure 2 illustrates this point clearly and indicates that a stretch factor might be used as a useful diagnostic for β. Notice that the variation of $[1-(v_x/c)]^{-1}$ with azimuth angle gives rise to an apparent rotation of the precession axis of either jet away from the line of sight to the observer. As an example, in Figure 2, for $\beta = 0.815$, the precession axis of the forward beam appears to be inclined at 90° to the line of sight, corresponding to a rotation of 50° from the true inclination of 40°.

We will define a stretch ratio f as the ratio of the angular distance from the source to features in the receding and approaching beams, respectively, which were ejected at the same time. Note with this definition f is normally <1 for

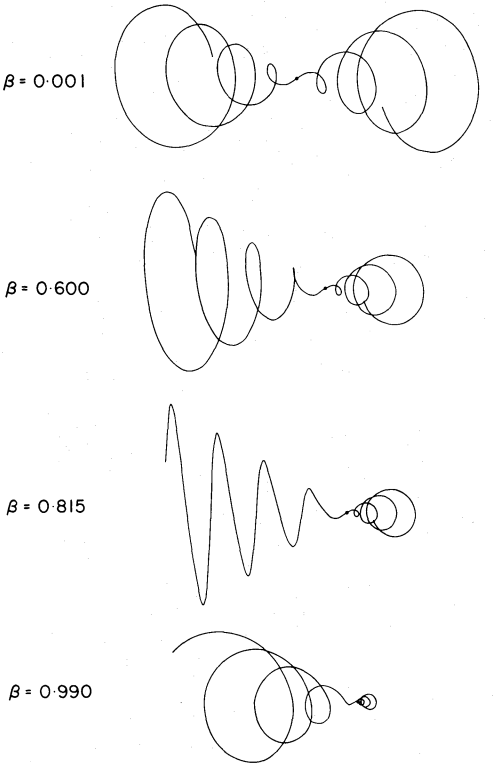

FIG. 2.—Geometry changes with beam velocity. Values of $\beta = V_{\rm beam}$ are shown. Models all have $i = 40°$, $\psi = 20°$, and $\theta = 0$. As β increases, the approaching beam is stretched and the intensity contrast between approaching and receding beams increases. Light time effects produce an apparent change in cone axis directions. At $\beta = 0.815$ the approaching cone appears exactly side-on.

small values of ψ. Combining equations (1) and (6) with the light travel time factor, we get

$$f = \frac{1-\beta\left\{\sin\psi\sin i\cos\left[\theta-\Omega\left({}_0t_1-{}_0t_{\rm ej}\right)\right]+\cos\psi\cos i\right\}}{1+\beta\left\{\sin\psi\sin i\cos\left[\theta-\Omega\left({}_0t_1-{}_0t_{\rm ej}\right)\right]+\cos\psi\cos i\right\}}. \tag{8}$$

For $\psi \leq 10°$, $f \approx (1-\beta\cos i)/(1+\beta\cos i)$. For larger values of ψ, the value of f will depend on the azimuth of ejection, $[\theta-\Omega({}_0t_1-{}_0t_{\rm ej})]$, and lie in the range

$$\frac{1-\beta\cos(i-\psi)}{1+\beta\cos(i-\psi)} \leq f \leq \frac{1-\beta\cos(1+\psi)}{1+\beta\cos(1+\psi)}.$$

The lower limit pertains to an azimuth of 0° which corresponds to ejection within the forward jet closest to the line of sight. We discuss this effect further in § III.

b) Image Intensity

We now consider the spatial intensity variations introduced in the image as a result of variations in the line of sight component of velocity for different parts of the jet and counterjet. We assume that the emission from each plasmon is optically thin at the frequency of observation with a spectrum in the rest frame of the plasmon of the form: spectral power emitted, $P(\nu) \propto \nu^{-\alpha}$. Following Ryle and Longair (1967) the flux density, $S(\nu)$, (W m^{-2} Hz^{-1}) of a moving plasmon is given by

$$S(\nu) = S_r(\nu)\mathrm{D}^{3+\alpha},$$

where D = Doppler shift factor $[\gamma(1-\beta\cos\phi)]^{-1}$,

$S_r(\nu)$ = flux density of an identical plasmon at rest and instantaneously at the same distance.

The actual intensity distribution expected for a particular model depends on the size of beam convolved with the array of plasmons and on assumptions regarding the temporal evolution of a plasmon with its proper age. In our model calculations we assume a constant rate of ejection of pairs of plasmons. Because of the stretch ratio f discussed previously, this gives rise to a higher plasmon density per unit area of sky in the counterjet than in the forward jet by a factor equal to the reciprocal of the stretch ratio. In addition, because the individual plasmons are assumed to be optically thin, intensity enhancements will occur whenever the line of sight is tangent to the trace of the jet.

To consider the effects of plasmon evolution, we assume that S_r decreases with the proper age ($\Delta\tau$) of the plasmon according to a simple power law of the form $S_r(\Delta\tau) \propto \Delta\tau^{-\delta}$. In this case $S_r(\Delta\tau) \propto (D\Delta_0 t)^{-\delta}$ since $\Delta\tau = D\Delta_0 t$.

$$\therefore S(\nu) \propto D^{3+\alpha-\delta}(\Delta_0 t)^{-\delta}. \tag{9}$$

We have nominally adopted a value of $\delta = 1$ as this is found to give satisfactory model fits to the data. We have included the factor $(\Delta_0 t)^{-1}$ as a linear spreading of plasmons with time. In view of the uncertainties in the plasmon evolution and the relative insensitivity of model intensities to it (compared with forward beaming and geometrical overlap), we do not develop this further in the present work.

c) *Effect of Cosmological Redshift and Relative Velocity*

We now consider the effects of a cosmological redshift and of a relative velocity between source and observer on the above conclusions. The simplest case to analyze is that of a relative velocity. Consider a second observer who is instantaneously coincident with the first observer but whose velocity with respect to the distant source is zero. The above analysis will then apply to this observer. However, as Penrose (1959) and Terrell (1959) have shown, the image seen by the first observer is simply related to that of the second observer. In particular, Terrell has shown that the first observer's image is simply a conformal transformation of the second observer's image. Since the image is small (less than a minute of arc), the conformal transformation results only in a change in size but no change in shape. Furthermore the relative *intensities* of various parts of the image will change (a) if there is a change of solid angle of that part of the image under the conformal transformation, and (b) because of the Doppler shift in the frequency between the two observers. The intensity changes due to (a) leave the *relative* intensities the same because the shape is left unchanged. The Doppler shift also leaves the relative intensities unchanged because of the assumed power-law nature of the spectrum.

The possible effect of the cosmological redshift can be analyzed in a slightly different manner. We will assume that the true time scale of any effects we are examining are much smaller than the Hubble time, and the size of the jets are much less than the radius of the universe. With negligible error, we will assume the spatially flat (critical density) Robertson-Walker model of the universe. The results for other cosmological models differ only by negligible terms, of order the diameter of the source as a fraction of the radius of the universe. This universe has a metric of the form

$$ds^2 = c^2\,dt^2 - R^2(t)\left(dx^2 + dy^2 + dz^2\right).$$

Define a new time τ by

$$\tau = R(t_0)\int dt/R(t),$$

where t_0 is the time corresponding to the occurrence of the phenomenon we are viewing. The behavior of light in this new coordinate system is identical to its behavior in flat spacetime. The equations of motion for a particle traveling out from the source in the absence of external forces become

$$dx/d\tau = V_0 R(t_0) c\left\{R^2(r)c^2 - v_0^2\left[R^2(t) - R^2(t_0)\right]\right\}^{-1/2}.$$

The particle velocity $dx/d\tau$ is no longer a constant but changes. This change occurs only over a Hubble time scale, however, and can be neglected for the sources we are examining which have a much shorter time scale.

We will define a hypothetical observer whose physical time was τ and whose spatial coordinates were $\boldsymbol{x} = R(t_0)\boldsymbol{x}$, and assume that $R(t)$ did not change appreciably during the time the jets were formed. This hypothetical observer

would see exactly the scene described above for the observer in flat spacetime. The true observer in time t differs from the hypothetical observer by only a scale factor $R(t)/R(t_0)$ for his time and distance. Since the observed image is an angular image, this image will not change under a change in the scale factor for distances. The change in the temporal scale by $R(t)/R(t_0)$ from the hypothetical to the real observer results in a redshift of all the frequencies emitted by the source. Again the scaling behavior of the power spectrum implies that the relative intensities of the various parts of the image will be the same for both the real and hypothetical observers. Since the hypothetical observer sees the same image as the flat spacetime observer sees, so does the real observer. The cosmological redshift therefore does not alter the appearance of the source.

III. MODEL FITTING: PROCEDURES AND DIAGNOSTICS

The models are fitted by inspection of intensity data, together with information on polarization, spectral index, and resolution. The basic model has variables i, ψ, θ, and β. In addition to the geometrical considerations and relativistic Doppler intensity enhancements, it is possible to model the aging of plasmons by allowing them to spread out with time and also by letting the spectral index change with time, measured in the plasmon's frame. These require two functions, each involving at least one variable. We can also allow the precession cone angle to vary with time, as measured by the central body. This too requires at least one more variable.

We restrict the above extra freedoms in the following reasonable ways: (1) the plasmon-spreading is close to linear in time and determined by observed widths and intensities, (2) the spectral index must lie within reasonable limits ($+0.5$ to -2.0, roughly) and in some cases it may be a measured quantity, and (3) the cone angle can only *increase* with time, never more slowly than linearly.

We have two modes of display: (1) geometry only, which is the principal constraint, tracing the beam center; or (2) intensity and beam-width simulation. This is a dot mosaic (see, e.g., Figs. 3 and 4) similar to that used by Icke (1981), indicating intensity by a linear blackening, and beam width by a Gaussian of width increasing as modeled. Because of the nonrigorous representation of beam width and intensity, we have not converted this to a more measurable form, such as contours. We believe this form of display allows us as much sensitivity in model-fitting as the model itself warrants. Finally, we can match observational resolution by setting the appropriate lower limit to the beam width as it is displayed.

The model clearly does not take account of variations in intensity or symmetry of the two-beam ejection, or interactions with a (stationary or moving) intergalactic medium.

It is clear that the principal parameters i, ψ, θ, and β can yield a bewildering variety of models. We therefore wish to consider general properties of models, and identify those more likely to be observed and/or recognized. While geometry is the most powerful diagnostic of a model, source intensity is generally the overriding observational constraint, with resolution a close second. We therefore consider first some geometrically-based grids and then look at the types of source most likely to be found in real data.

In Figure 3 we present a grid of models for two different cone angles ψ and values of β, covering all angles of inclination, i. This gives an impression of the range of geometries which might be encountered. $\theta = 0$ has been used in all these models; similar grids could be generated for other orientations. To see the effect of changing θ, Figure 4 shows a particular model with θ varying by steps of 60°. Familiarity with this diagram helps to visualise the rotations possible in Figure 3.

An important aspect of recognizing and modeling observations is the intensity variation in the pattern. This depends on the model itself, and the resolution and dynamic range of the observations. Figure 5 shows the same model seen with various resolutions and sensitivity, and it is clear that the appearance changes greatly between them.

One general point is that if the observed source structure is curved and is very symmetrical, the jet velocity *must* be low. As the velocity is increased, the geometry of the source and intensity distributions change quite rapidly. If the cone axis is exactly in the plane of the sky ($i = 90°$), this effect is minimized, but even for a moderate cone angle ($\psi = 20°$), distortion of the structure will occur (see Fig. 3). Thus the Z-shaped sources NGC 326 and 3C315 are bound to be low velocity by their symmetry, while we may suspect that some of the one-sided jets have high β values.

As mentioned in § II, the principal geometrical effect of β is in the stretch ratio f (eq. [8] and following). This can be put into practical use as a diagnostic most easily by measuring the distance along the projected cone edge of the pattern to identifiable, symmetrically opposite features. In Figure 6 we show how the ratio depends on β and i. The left-hand panel shows the values for small ψ. The right-hand panel shows how the family of curves drops as ψ becomes larger (when $\psi > i$, the cone edges are not defined and the ratio f is not simple to measure). As ψ increases the cone edge corresponds to azimuth values which approach 0 from $\pm\pi/2$, and, as pointed out in § II, this corresponds to a decrease in f. These curves are empirically derived in order to approximate more closely the process involved in model fitting. However, the general relationships in Figure 6 hold for *any* double beam (precessing or not) with a kink or feature which appears in both curves.

1982ApJ...262..478G

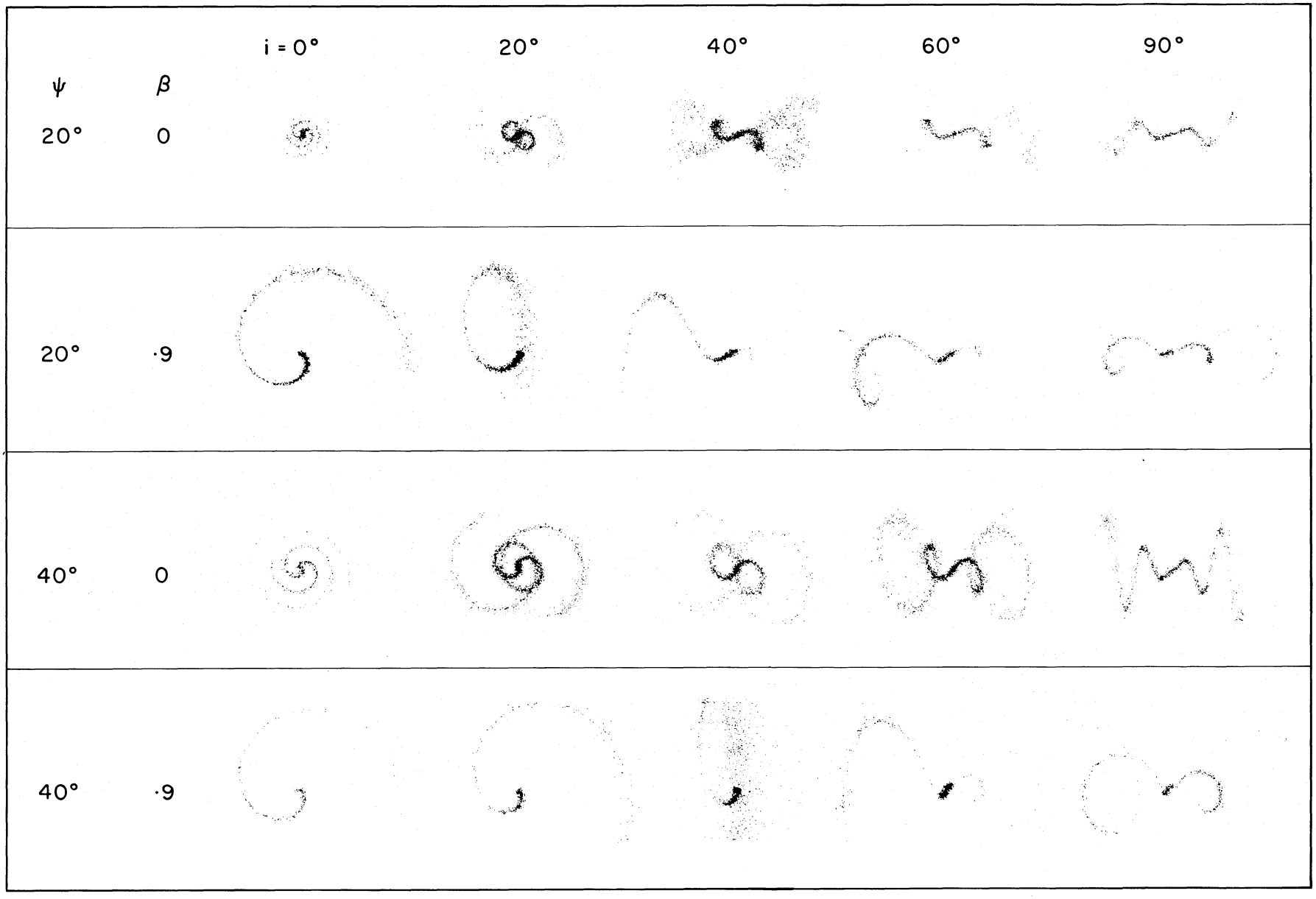

FIG. 3.—A family of models to show the effects of inclination i, cone angle ψ, and jet velocity β. For all these models $\theta = 0$, i.e., the direction of ejection at the source, along the edge of the cone, is as close as possible to the observer's line of sight, at an angle $(i - \psi)$. (When $i = \psi$ therefore, one is looking straight down the jet at the core.) Note that since all orientations of the cone axis in the sky are equally likely, the probability of observing these structures will increase toward the right, ignoring other selection effects.

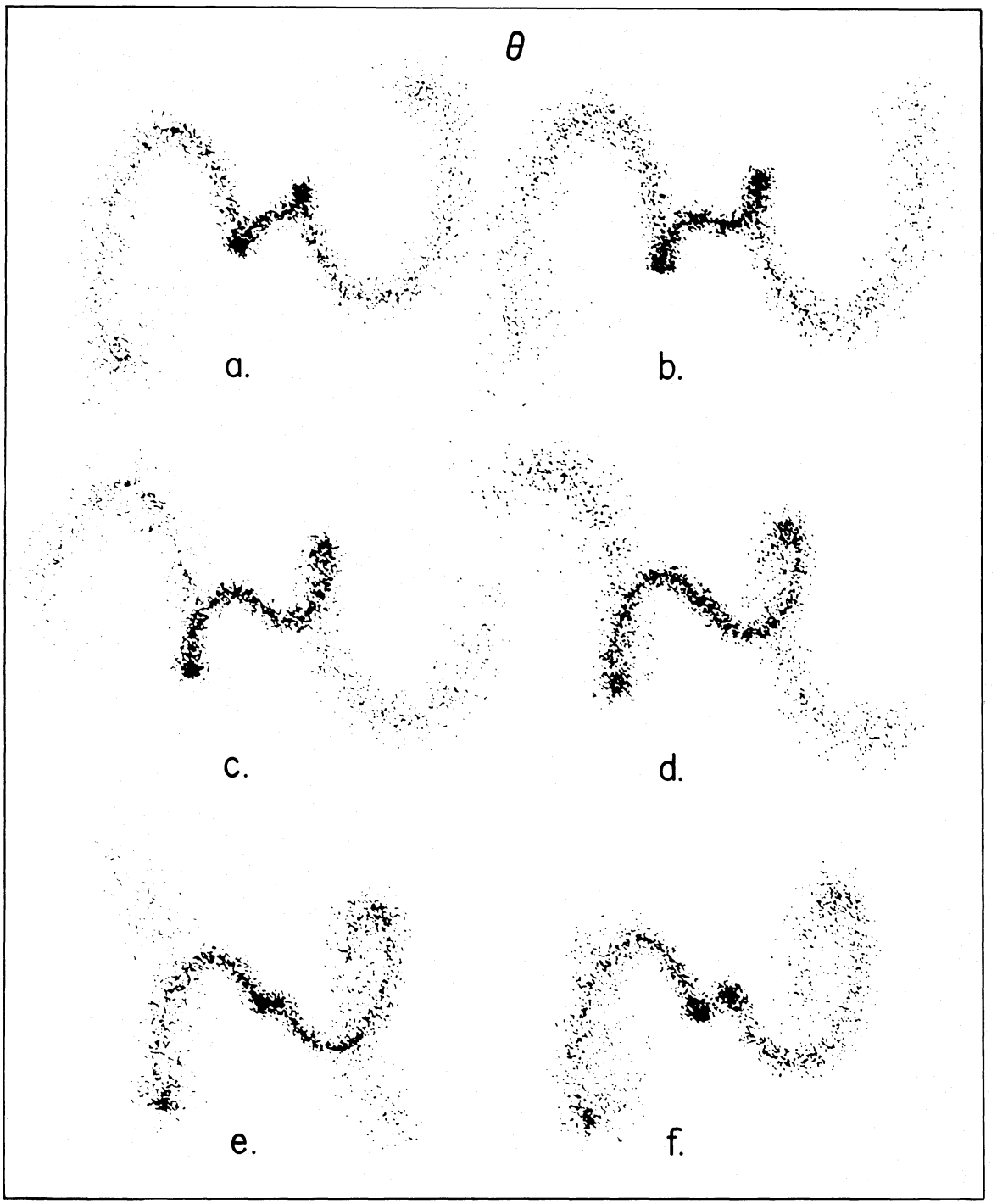

FIG. 4.—One rotational cycle (60° intervals) of a model: $i = 60°$, $\psi = 30°$, $\beta = 0.1$. Jet ejection is nearest the line of sight in (d). Right-hand beam is approaching. Density of dots is directly proportional to source intensity.

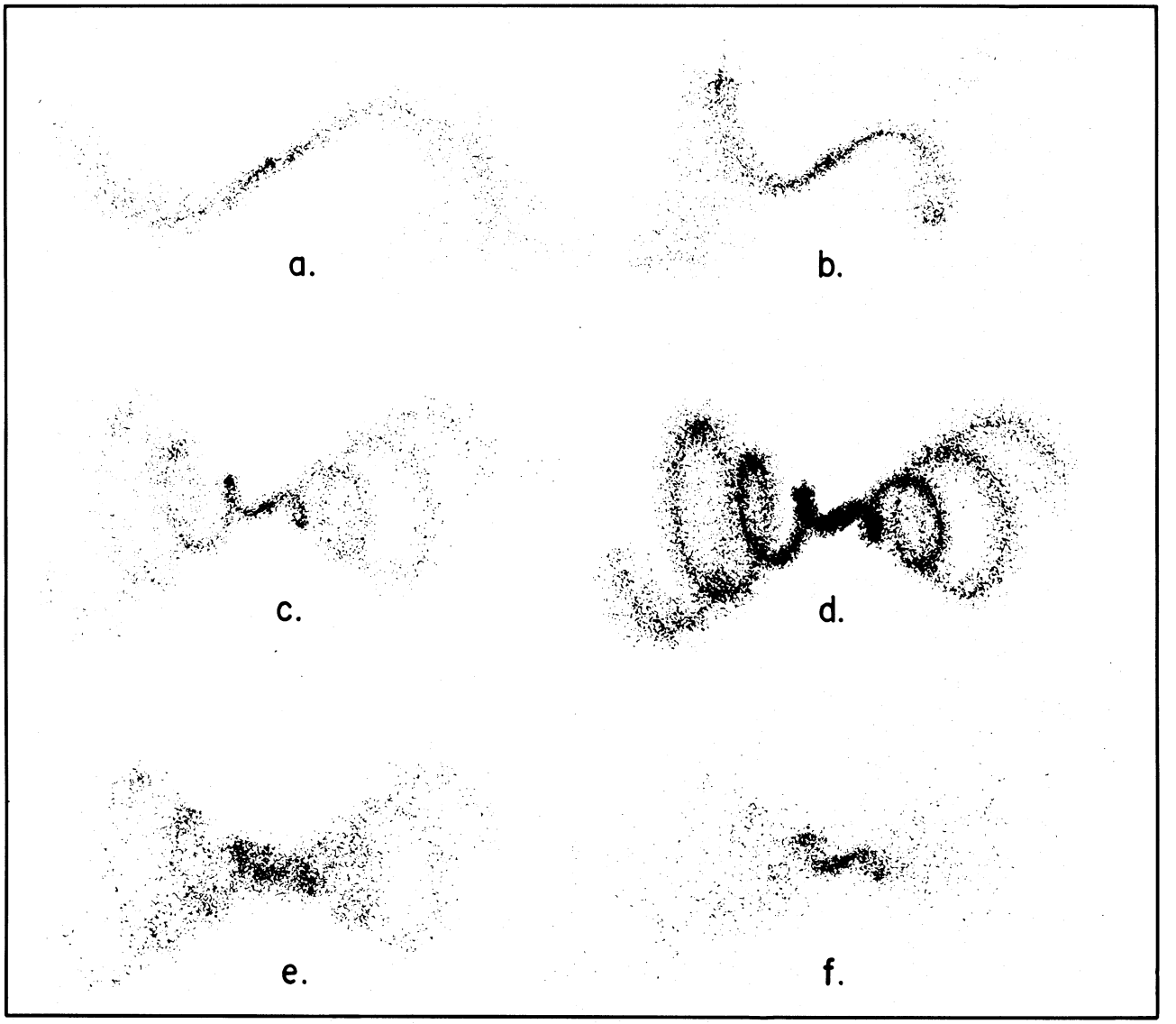

FIG. 5.—The same model under different observational conditions. $i = 60°$, $\psi = 25°$, $\beta = 0.2$. (*a*)–(*c*) show different resolution and field sizes. (*d*) shows (*c*) with a higher dynamic range. (*e*) shows (*c*) with a 3 times larger beamwidth. (*b*) shows (*c*) with a 4 times more rapid dispersal of plasmons into the surrounding medium.

Figure 7 shows a family of models of very relativistic jets ($\beta > 0.9$) where i is close to or equal to ψ so that part of the structure is pointing directly toward us (or nearly so). While these are not necessarily more common, they are very likely to be observed since the brightness enhancement is very high. We have chosen $\beta = 0.9$ for all the models, but the geometry of the observed structure is not very sensitive to β although, of course, the linear scale and intensity enhancements would be. The observed shape is, however, very sensitive to θ (the orientation) and models for $\theta = 0$, 120°, and 240° are given in adjacent columns. The first row shows the structure for a half-cone angle of 17° with the line of sight still 6° outside the cone ($i = 23°$). The second row shows the same cone angle with the line of sight along the edge of the cone ($\psi = i = 23°$), and the third row shows the same situation but with a larger cone angle ($\psi = i = 57°$). The bottom row shows how the structure in the row above is affected by allowing the cone angle to increase with time, an effect which was found to be necessary to fit some of the models in the next section. The value at the center is $\psi = 57°$, but the structure further from the center (emitted at an earlier time) is appropriate to steadily smaller cone angles. Note in particular the displacement of the source from the brighter part of the structure in some of these models.

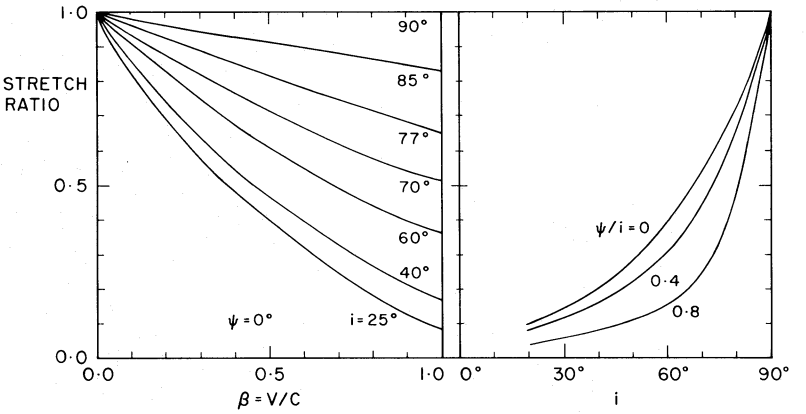

FIG. 6.—The left-hand panel shows the "stretch ratio," the ratio of distances from the central source to similar pattern features in the receding and approaching beams, measured along the projected cone edge, as a function of $\beta = v_{\rm beam}/c$. This family of curves is for $\psi = < 10°$. As the cone angle increases, the family of curves drops in the diagram. To estimate this effect, the right-hand panel shows the stretch ratios at $\beta = 0.9$ for different ψ/i ratios. For patterns with $i > \psi$ and β low enough for both sides of the structure to be seen, the ratio is easily measured, together with an upper limit for ψ, enabling good estimates to be made of i, ψ, and β.

IV. PROBABILITY OF OBSERVING THESE STRUCTURES AND OBVIOUS SELECTION EFFECTS

The probability of orientation of source axis at any angle to the line of sight must be random and therefore the actual number of sources with their axis at any particular angle to the line of sight must vary as $\sin i$. However, the chance of detecting these structures must be deeply influenced by selection effects. Certain orientations will be particularly favorable:

1. Relativistic cases in which $i = \psi$ and $\theta = 0$, i.e., the emission from the quasar is directed along the line of sight at the core. This then gives a bright, Doppler-enhanced, possibly flat-spectrum core coincident with the QSO. These are, therefore, sources which will tend to be observed in a high-frequency survey, if the beams are truly relativistic. The extended emission may lead to an asymmetric, curved structure (e.g., Fig. 7, row 2, col. 1) with the QSO at one end, a structure noted in a number of quasars (e.g., some of the D2 quasars (Miley 1971) and the C-sources (Readhead *et al.* 1978) and already suggested to be the result of precession (e.g., Linfield 1981). For a larger cone angle or higher value of β, the extended structure may lead to a banana-shaped structure (Fig. 7, row 3, col. 1) dominated by the Doppler-enhanced parts of the structure pointing nearly along the line of sight. In the next section we suggest two sources which may be of this type.

2. Any case in which the emission from the central object is directed toward the observer within the beaming cone of half-angle $\sin^{-1}\gamma^{-1}$ [where $\gamma^2 = 1/(1-\beta^2)$] so that the central object still appears bright. This will be less restrictive for low β sources than case (1) above (for $\beta = 0.7$, angle $\sim 46°$), although the enhancement will of course be less if β is low. Since the central source will still be bright even if the cone axis is at an appreciable angle to the line of sight in these cases, a common feature of the large-scale structure will be "knots" or "commas" well away from the central object where the radio emission is enhanced both by Doppler boosting *and* by projection effects.

Since we do not know the distribution of β or ψ among the quasars we have not attempted to estimate these effects quantitatively. Furthermore, we do not know if, in addition to the relativistic structure, we may add a further point radio source at the position of the quasar. We note that in our fitted models, this seems to be the case in several sources.

Many of the listed quasars have been found in the optical identification of flat-spectrum and/or variable radio sources detected at 2.7 or 5 GHz. Since these are presumably the relativistically enhanced ones, they provide us with a suitable list for searching for structures of this kind. In particular, any displacement of the optical position from the maximum intensity of the radio structure would be very important in pinning down the model. Also high-dynamic range maps of "short bent jet" sources to search for the much weaker pattern which should be present in a precessing object would be a test of these models.

V. SOME DETAILED MODELS FOR OBSERVED RADIO SOURCES

In this section we first present our best models to fit the observations of six radio galaxies and quasars. The model for 4C 18.68 is shown in Figure 8 and models for five other sources in Figure 9. Each source is discussed individually in

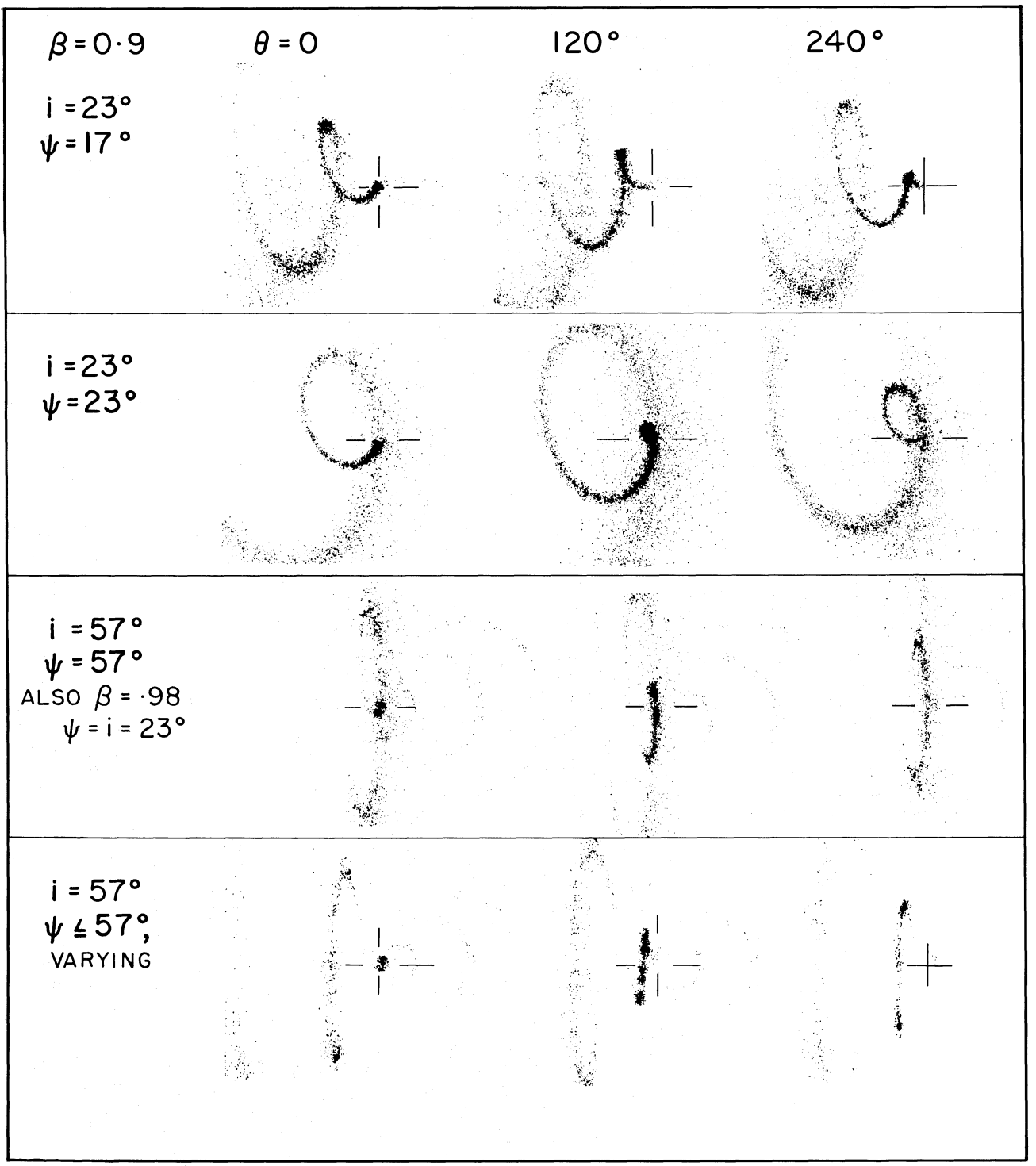

FIG. 7.—Models of high jet velocity ($\beta = 0.9$). In these cases, approaching (left-hand) beam is far more intense than the receding beam. The grid is arranged to allow easy mental interpolation. The extreme intensity enhancement makes these models likely to be observed. In the lower panel, ψ increases in time to a current value of 57°. QSO positions are indicated with lines. Note the cases where the QSO position is displaced from the maximum intensity of the jet. Note also that an increase of β has the same effect as an increase of i and ψ as in lines 2 and 3.

1982ApJ...262..478G

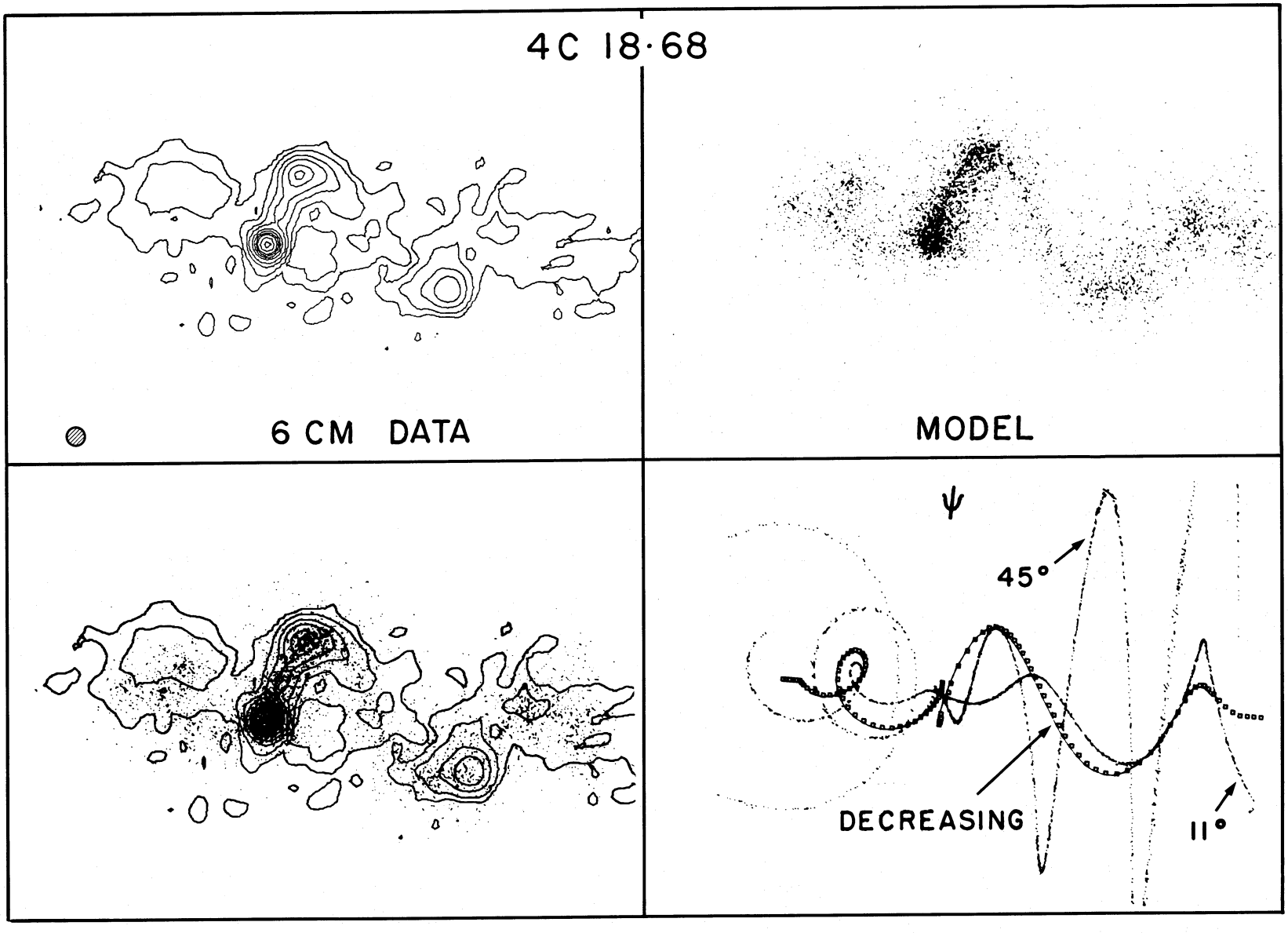

FIG. 8.—Data and models for the quasar 4C 18.68. Parameters appear in Table 1. Lower right-hand panel shows how ψ must increase to fit the observed geometry. Curves are shown for cone angles of 11° and 45°, together with the suggested model (*line with dots*) where ψ increases nonlinearly toward the center of the structure. The dots are at equal intervals of θ at the time of ejection. The observing beamwidth of 0".4 is shown in the upper left-hand panel.

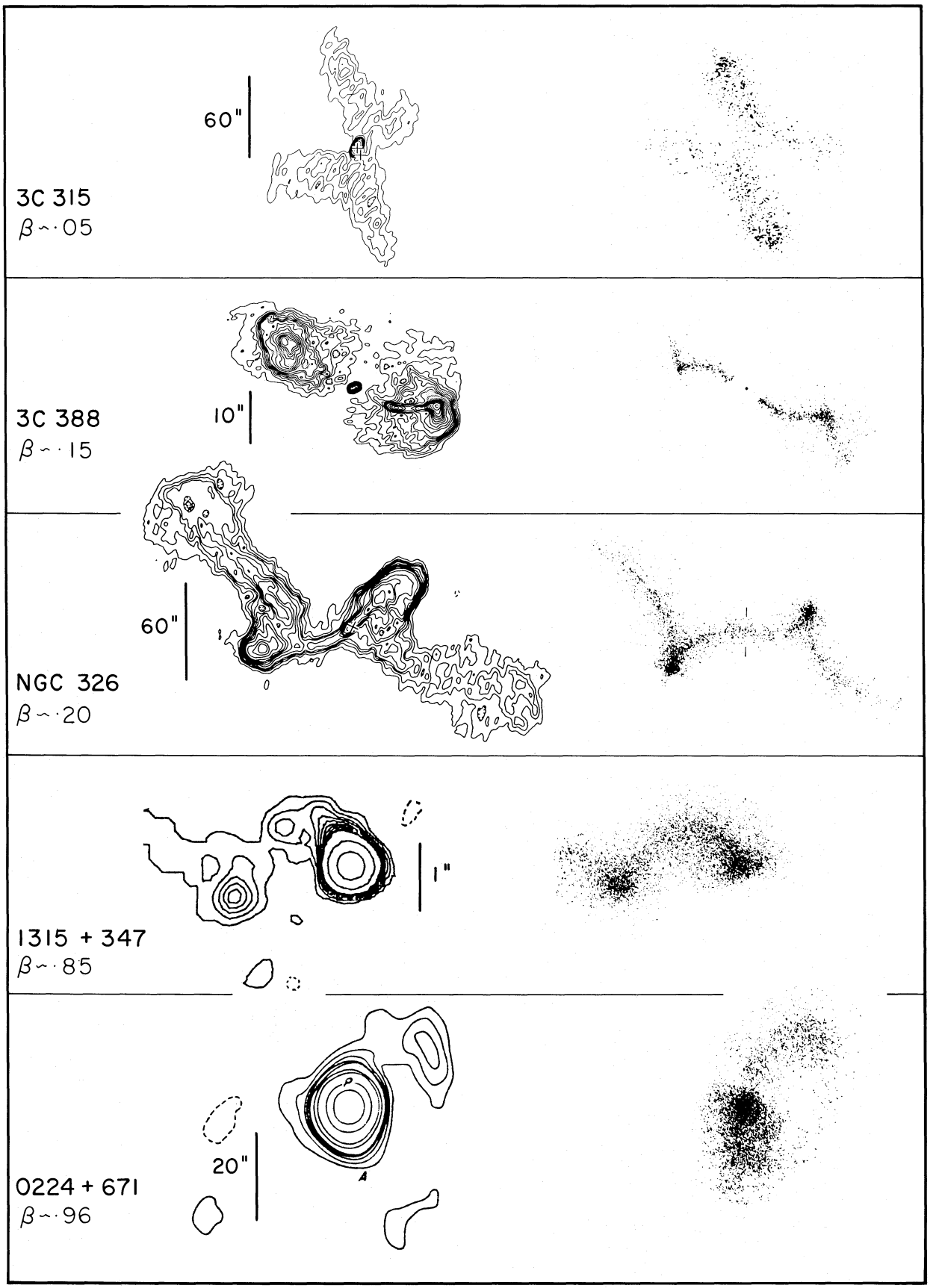

FIG. 9.

TABLE 1

PRECESSING JET PARAMETERS FOR 10 SOURCES

Object	z	i[a] (degrees)	ψ[b] (degrees)	β	θ[c] (degrees)	P(yr)	Remarks
3C 315.....	0.11	17±15	<17±15	0.05±0.05	230±15	$\sim 10^7$	$\psi = 0$ at >1 turn
3C 388.....	0.09	37(to 45)	6(to 12)	0.15(to 0.20)	−200±10	5×10^5	ψ constant
NCG 326 ...	0.05	23±10	<23±3	0.20±0.08	170 ~ 10	10^6	$\psi = 0$ at 1.5 turns
4C 18.68	0.31	60±10	<80±6	0.70±0.05	−75±30	4×10^4	$\psi = 0$ at 2.5 turns, $\alpha = 0.3$ to -1.5
1315+347 ...	1.05	20±4	<25±4	0.85±0.05	75±30	9×10^3	$\psi = 0$ at 2 turns, $\alpha = 0.2$ to -1.1
0224+671 ...	...	14(to 34)	14(to 34)	0.96(to 0.80)	80±40	(3×10^4)	ψ constant, $\alpha = 0.2$ to -0.8
1730−130 ...	...	(<)35	(<)35	(>)0.8	0±20	5×10^4	1.5 turns only
0945+408 ...	1.25	17±11	23±11	0.9±0.05	0±20	1.6×10^4	$\psi = 0$ at >5 turns
0716+714 ...	...	45±6	35±8	0.6±0.1	140±45	(10^5)	$\psi = 0$ at >1.5 turns
0707+876 ...	...	(<)11	(<)4	0.3±0.1	140±35	(10^5)	...

[a]Acute angle.
[b]Half-cone angle of precession. Where ψ increases with time, present (max) value is given.
[c]Positive rotation is clockwise in approaching beam.

the text. Table 1 contains all the model parameters. Finally, we fit and discuss briefly two types of structure which may be quite common among compact core QSOs and show how they may arise if the beam is relativistic.

4C 18.68. The data for this object are described in Gower and Hutchings (1982, hereafter GH) and are shown in Figure 8. The main characteristics of the structure are the two bends to the W of the source, the continuity of the structure suggested by both intensity and polarization, and the faintness and lack of detailed structure to the E of the source. As already mentioned by GH, the geometry requires the W side to be approaching, the line of sight to be outside the cone, and a fairly relativistic velocity. In this case, precessing models are fairly closely defined by the geometry. The known spectral indices and intensity ratios are also consistent with the geometrical model.

Figure 8 shows the 6 cm data and model displayed with the same resolution. It is also shown in the figure that the data cannot be well described with a single cone angle, and that an increase of this angle for matter close to the source is indicated. While it is undesirable to introduce further parameters, in this case it is necessary and we can think of no other parameter which would improve the fit. It is also possible to derive information on *how* the angle increases, from model fitting. The angle must increase nonlinearly with time (at the source) near the beginning of the precession, unless interaction with a medium has affected the outer parts of the jet.

The intensity is enhanced where the beam is (*a*) compact, (*b*) directed toward the observer, and (*c*) showing projection effects when it is not in the plane of the sky. The bright spots in the model arise in all three ways, and the model we adopt has the best combination of geometry and intensity. The intensity evolution also depends on the change of α with plasmon proper time (position), but in this model, that is constrained by the observations, since the distribution of α with distance from the central source is known (see GH). The polarization vector behavior is also a guide.

From the point of view of intensity, there is no particular need for a source other than the relativistic beam itself at the location of the quasar. However, if this is in fact the case, the exact position of the central source, the optical QSO, is of interest in defining the model. If the cone angle becomes large enough, the line of sight lies just within the precession cone near the QSO, and the QSO is at or even W of the brightest point (A). If the cone angle does *not* exceed the inclination of the line of sight to the precession axis (i.e., the line of sight is always outside the precession cone), the QSO lies E of A. Our best model (Fig. 8) has the source somewhat N of A. The best optical QSO position lies E of A, but within 1 σ of it and of our model position. Thus, it becomes evident that optical positions known to 0".1 or 0".2 would be useful in testing or refining such models. They would also be useful in general in spotting objects of this nature whose structure is not as well defined.

FIG. 9.—Observations and models for five sources for which parameters are given in Table 1. The source centers are lined up in a uniform grid. The upper three are radio galaxies and have low values of β. The lower two are QSOs with $\beta > 0.85$ and emission from the jet detected on only one side of the QSO. In the slower moving jets, interactions with the IGM are more likely to occur and may explain shortcomings of model fits. Lobes around 3C 388 jets can be made if some of the jet matter disperses much more rapidly than the rest as shown in the model. The model beamwidths have been chosen to match the data. See text for further discussion of individual sources. Observational data for 3C 315, NGC 326 from Fomalont 1981; 3C 388 from Burns and Christiansen 1980; 1315+347 from Perley 1981; 0224+671 from Perley *et al.* 1980.

The model we present is summarized in Table 1, and we feel that it fits the data remarkably well. If we accept the model, we should consider its implications. The object 4C 18.68 lies in a group of objects which may be associated with it (Yee 1981), and is surrounded by a very large radio halo ($\sim 20''$). The whole scenario is suggestive of a recent history ($< 10^7$ yr) of activity which has culminated in the precession of a double beam, lasting only two or three cycles. The implied precession period is 4×10^4 yr. The present situation then corresponds to that close to the end of the process, since the precession angle will reach 90° within one cycle. At that time, either a binary merger will occur, or the jet will continue to rotate in the plane normal to its original direction. (In this connection, we may note that Heckman *et al.* 1982 have decided that this is the case for 3C 305). The energetics of that situation also indicate that it cannot last more than a cycle or two, unless ejection is no longer controlled by the angular momentum of the central body.

One may wonder at the probability of seeing what seems to be a special and short-lived chapter in the quasar history. We suggest that two circumstances select it for discovery: (1) the lifetime of the process may in fact be comparable with the duration of the quasar's present active epoch, being fuelled by the capture event we are observing (see Stockton 1982); and (2) the source geometry makes it a strong radio source in our line of sight (among low-z objects). It seems in any case to be the best example in a small sample of objects, so that it is not immediately obvious that it is too special a case to be seen.

1315+347. This is a QSO whose radio structure has been mapped by Perley (1981). As shown in Figure 9, its structure bears considerable resemblance to 4C 18.68, reversed E to W. Thus, not surprisingly, a similar model fits it well. Here too, the cone angle must be increasing rapidly and will reach 90° in little more than one more cycle. The best fitted model for this source has a high β value (notice that no receding beam is seen at all) and a small angle (20°) to the line of sight. The precession axis in the model is at a small inclination to the line of sight, again suggesting beaming selection effects in radio QSOs.

The projected cycle length of 11.3 kpc ($z = 1.05$) gives a cycle period of only 8500 yr. For β values between 0.8 and 0.9, the period changes by a factor of ~ 2, but even with this uncertainty the period is remarkably short. In fact, in 10 yr the bright knot E of the source should move by $\sim 0''.002$. Such rapid changes in position and position angle suggest the possibility of measuring them directly with VLBI techniques.

0224+671. This is one of the structured sources observed by Perley, Fomalont, and Johnston (1980) with the incomplete VLA. The structure is suggestive of the models in Figure 7 where the line of sight lies near the cone edge. We find that we can fit the data satisfactorily as shown in Figure 9 with the model given in Table 1. As seen in Figure 7, there is a degeneracy between angle and β value, and this also is indicated in Table 1. The shape and intensity distribution are well represented by the model, and it is important to note that some of the most characteristic contours are the faintest ones. The model requires only $\sim$ one turn (probably since the data have less detail), and there is no requirement or indication that ψ is varying. The source redshift is not given by Perley *et al.* but since (for $H_0 = 100$, $q_0 = 0$) the scale in kpc arcsec^{-1} is a maximum for $z \sim 1$ and the luminosity makes it unlikely that $z < 0.05$, we can still set limits to the deduced precession period. These are $6 \times 10^3 - 10^5$ yr with a "most probable" value of 3×10^4 yr, very comparable with the values for the two other QSOs we have modeled.

3C 388. This source, associated with a cD galaxy at $z = 0.09$, has been discussed by Burns and Christiansen (1980). The radio structure has two outer lobes and an intense curved jet in the western lobe (Fig. 9). We point out that the eastern lobe also contains a central ridge, less well defined, but which is a remarkable inverted image of the western jet.

The data on this source thus resemble a sideways-on double jet with a small cone angle. The intensity distribution indicates a low but significant β value. The source parameters can be derived fairly satisfactorily by reference to Figure 6. The stretch ratio from the source geometry (Fig. 6) is ~ 0.8, and the opening angle of the peak intensity jets means that $\psi < 9°$. From Figure 6, we can see that the geometry will fit models from $40° < i < 80°$ and $0.15 < \beta < 0.5$. At $i = 40°$, ψ must be $\sim 5°$. The relative intensities of the approaching and receding beams require the low β end of this range. Figure 9 and Table 1 show our best fit model based on the full model comparison.

The source has several notable features. First, the lack of signal near the source, which seems to indicate (or is consistent with) cessation of ejection in both directions at about the same time. In our model we have made this abrupt turnoff. Second, the existence of bright spots which are not given in a uniform ejection model. The principal ones are beyond the kink in the receding (E) arm and near the inner end of the approaching (W) arm. It is possible that the enhanced emission is seen at places which are periodic and interleaved on alternate sides, i.e., the beam is enhanced periodically on alternate sides. This behavior has been noted in a number of radio sources by Rudnick (1982). If so, the ratio of that period to the precession period in 3C 388 is about 4 to 1.

The third feature of 3C 388 to note is the extended halo around each arm of the double jet. Our model in Figure 9 has allowed some of the plasmons ($\sim$ one-third) to spread ~ 4 times faster than the rest. This improves the resemblance between model and data but may not be relevant.

The overall fit to the data is good enough to make the model worth serious consideration. We note that Burns, Christiansen, and Hough (1981) do not favor relativistic Doppler projection effects, although we find that this effect

does account well for some features of the intensity distribution. They do, however, suggest that there is intermittency and asymmetrical small scale structure.

While only a small part of a cycle is seen in the pattern, it is clear that the model does not require a changing cone angle. A full cycle in the approaching beam would be roughly 25 kpc long, projected on the sky ($H_0 = 100$, $q_0 = 0$). With the i and β given for the model, a period of $\sim 5 \times 10^5$ yr is indicated. (For $i = 6°$, $\beta = 0.5$, $P = 1.3 \times 10^5$ yr.)

NGC 326. This source has very suggestive rotational symmetry and is another obvious candidate for our model fitting. Ekers *et al.* (1978) suggested precession for this source, though their model involved illumination of an obstructing wall of material by a straight jet rather than the unimpeded trail of a jet in our model. The radio emission of this source is associated with a cD galaxy positioned as shown in Figure 9, which has a redshift of $z = 0.05$.

The basic source shape is characteristic of a conical spiral viewed near to end-on and can be assessed for parameters using Figure 6. The stretch ratio is ~ 0.6, for which β lies in the range 0.2 upward for $i = 25°$ upward. The outer curvature and loops or cusps require i to be small, while the intensity ratio requires β to be small. Thus $i = 25°$ and $\beta \sim 0.2$ are good values. The intensity ratio is consistent with the geometry in making the E arm the approaching one. The values of i and ψ for our model agree well with those suggested by Ekers *et al.* (1978).

In fitting the details of the model, two things become clear. Firstly, the decreasing curvature of the outer arms can only be fitted with a cone angle that is initially small and then increases to give the prominent loops. In fact the geometry defines the model quite strongly. Secondly, the data clearly contains an overall U-shaped distortion, which the simple precessing model cannot match. The sweeping back of the outer arms and twisting of the SE loop from the best precession model are consistent with the effects of a force directed almost due N on the whole system. Aside from this latter point, which is not at all unlikely for a source in a cluster, we feel that the model gives a good fit to the data, generally consistent with the predictions of geometry and intensity.

The full cycle is estimated to be $\sim 2'$ on the sky, which indicates a precession period of $\sim 10^6$ yr.

This object is discussed by Wirth, Smarr, and Gallagher (1982), who suggest that its radio structure is the result of a single direction change caused by a close passage of the galaxy now some 60″ south of the active one. This is a valid concept and needs to be developed into a quantitative model of the radio intensity distribution to see whether it differs fundamentally from ours.

3C 315. This is a final low β source, which has a similar intensity and geometrical symmetry to NGC 326 (Northover 1976; Fomalont 1981; Högbom 1979). This source, in some ways similar to NGC 326, has a high degree of geometrical symmetry, with a stretch factor close to 1. The southern extensions are somewhat brighter and larger and presumably are the approaching parts of the ejecta. Both the symmetry and high curvature of its outer arms suggest a low i and low β. Figure 9 shows the best fit model. A family of models of low i and lower ψ fit equally well, with $\beta < 0.1$. The geometry of this system is constrained by the high curvature of the arms and the direction of the loops, which tend to pull the parameter ψ in opposite directions. The only way to achieve both is to have i and ψ both low (as low as 3°). This suggests that selection effects are at work again if the model applies.

We judge β to be > 0.05 to cause the intensity ratio observed, which yields a precession period of order 10^7 yr. If β is very small and intensity variations are due to inhomogeneities, the period and age of the plasmons must be very large.

The last two models described are examples of Z-shaped sources. Others are known and should be considered candidates for this type of model. Examples are the object 0847+491B (Machalski 1981) and 3C 196 (Lonsdale and Morrison 1980). NGC 315 (Fomalont 1981) could be fit as the inner part of a Z-shaped source, with a stretch ratio ~ 0.5.

Bananas and Commas. Certain orientations and features are particularly favorable for observation, as mentioned in the last section. Here we present two structures (in addition to the asymmetric, short, curved jet) which we feel signal the presence of relativistic jets and suggest models, although a detailed model is not as convincing in these cases due both to insufficient data and to the fact that at high β it is difficult to distinguish between the effects of β and of ψ.

a. Figure 10 shows maps of 0945+408 and 1730−130 (NRAO 530) (Perley, Fomalont, and Johnston 1980) and models which give about the same appearance for the large-scale structure, seen with fairly low resolution. In 0945+408, i is a little less than ψ so that the line of sight lies just inside the precession cone and $\theta = 0$, so that the source is pointing directly towards us at the core. In NRAO 530, $i = \psi$ and β is high so that the central source (again with $\theta = 0$) lies in the center of the extended structure. We speculate that there may be other sources of this shape and note that 2 or 3 of the maps of BL Lac objects shown at IAU Symposium 97 by Stannard (1982) showed this general shape, suggesting that in some BL Lac objects we are indeed looking right down the core of a very relativistic source. The large-scale structure is faint, however, relative to the central component so that the core itself may be an intense, beamed compact radio source in addition to the relativistic jet.

b. Figure 10 also shows maps of 0707+476 and 0716+714 (Perley Fomalont, and Johnston 1980), showing asymmetric structures. The models given here have i just outside ψ as in the first row of Figure 7 and β high—another

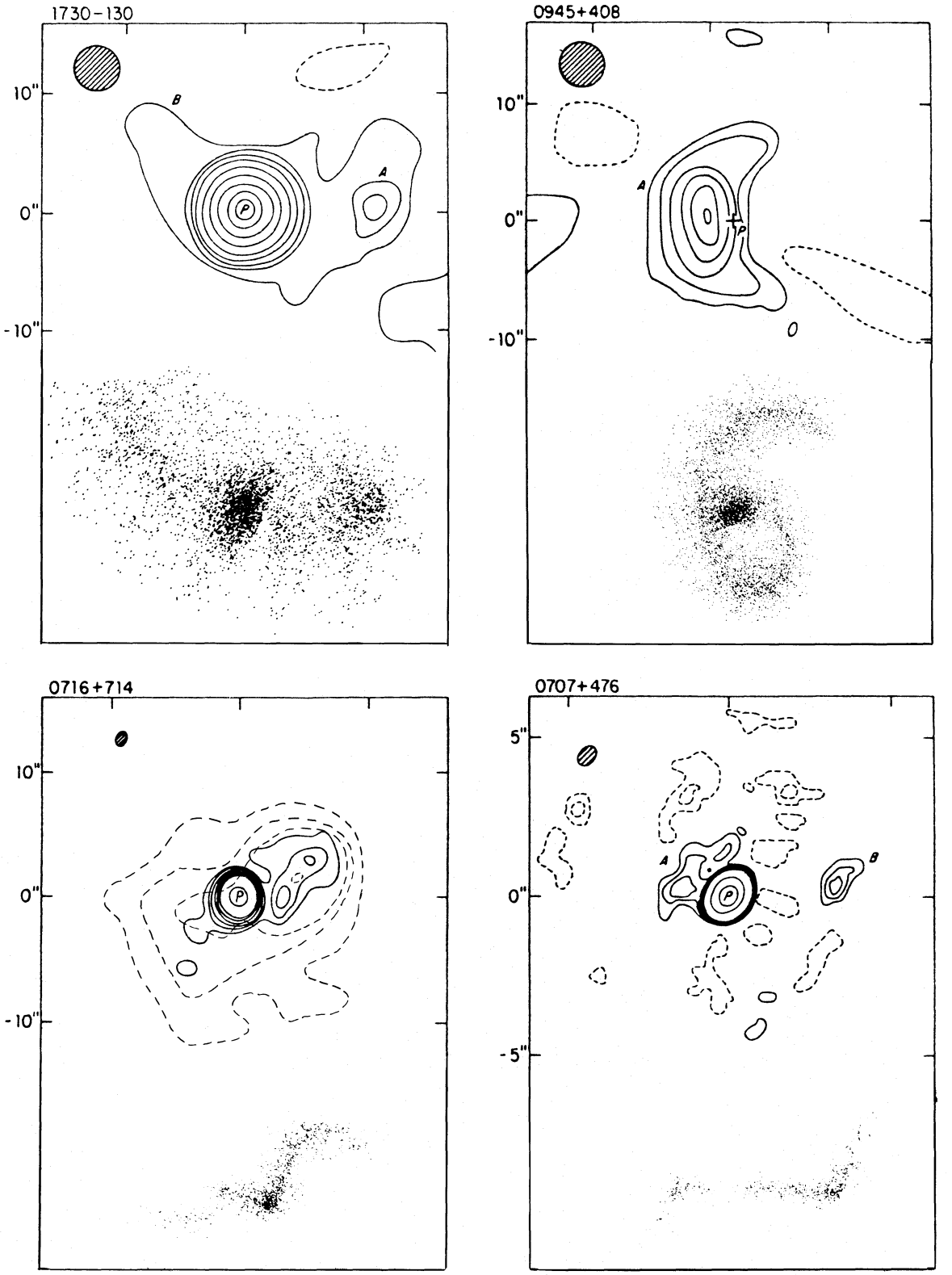

FIG. 10.—Observations and possible models of four sources from Perley *et al.* 1980 which have less detailed data. Upper two are "banana" sources in which the line of sight is near the edge of the precession cone. Lower two are "commas," in which enhanced radiation is seen detached from the source in data of low dynamic range. Models have spatial resolutions to mimic the data, and sources lie in a rectangular grid. In these sources, a central point source must be added to the jet model. In 0945+408 this point source has been removed from *P* in the data. 0716+714 shows both 6 cm and 20 cm data. Model parameters are given in Table 1. Horizontal and vertical scales are the same.

favorable orientation for seeing a bright central source, although in this case the best fit is not for $\theta = 0$. In these we wish only to point out that this type of "comma" displaced from the central source arises often in these models and may easily appear isolated if β is high, or in data of low dynamic range. Note that in the models in Figure 10 we require a flat spectrum point source at the jet origin, above that given by the model. The models in Figures 8 and 9 are already bright at or near the QSO, so that the adoption of a central optically thick source would be less obvious.

Discussion of Fitted Sources. Two features common to all the structures described above stand out. First, only about one cycle of the precession or rotation is seen in these quasars and radio galaxies. This is also true for SS 433, and in this case, since we know it continues to precess, it suggests that losses during the expansion of the material quickly make it undetectable. However, in the case of the extragalactic sources, it may be that the central object *only makes one or two turns*, often with an increasing cone angle, before dying.

Secondly, one does not see the classical double radio "lobes" beyond the relativistic structures in any of these cases except perhaps in the case of 3C 388. This again suggests that the sources have only recently become active (or that the nature of the jet is very different).

Finally, we feel that the lack of intermediate values of β in our examples is almost certainly a selection effect: the three radio galaxies (all 3C sources) were selected quite differently from the quasars, most of which appear in high-frequency surveys. As mentioned before, if the explanation suggested by Scheuer and Readhead is correct (that the radio-loud quasars are the ones that are relativistic and beamed toward us), then *these* are the ones which will tend to have the relativistic large-scale structure. The quasar with the lowest value of β, 4C 18.68 ($\beta = 0.7$), was selected at low frequencies and has only a faint flat-spectrum component. We suspect that the intermediate β structures are among this sample and have not yet been mapped with arc-second resolution. Several of the structures mapped by Neff (1982) around quasars in fact suggest lower β values (stretch ratios nearer to 1 and both beams bright), if they are precessing jets.

VI. DISCUSSION

We have presented precessing twin-jet models for several quasars and radio galaxies which fit the data well and show a range of bulk jet velocities from $\beta \sim 0$ to $\beta \sim 0.96c$. The existence of jets in active galaxies is well accepted from a variety of studies, both observational and theoretical. If relativistic beaming is indeed an important process in explaining the emission from the core of QSOs, it is probable that the large-scale structure of some quasars will be determined by relativistic jet velocities too, as we have found. The phenomenon of jet precession has been forcefully drawn to our attention in the object SS 433 which is generally considered to contain a compact object with a luminous accretion disk (e.g., Crampton and Hutchings 1981). In the following discussion, we invoke the generally proposed scenarios for QSOs of an accreting massive black hole.

Morphological studies of nearby QSOs (Hutchings *et al.* 1981; Hutchings *et al.* 1982; Wyckoff, Wehinger, and Gehren 1981; Yee 1981), all indicate a high proportion of asymmetrical or disturbed nebulosities surrounding QSOs, and there are several cases where galaxies are clearly interacting. All nearby QSOs appear to be members of small groups or clusters of galaxies (Stockton 1978; Yee 1981). These considerations have led Stockton (1982) to suggest that the QSO phenomenon is related to close encounters between galaxies, at least in the recent (low-redshift) objects. This is a very plausible way of feeding a large amount of matter into a central black hole long after the bulk of the primordial-galaxy gas has been consumed.

If we accept this very plausible scenario, it follows that some of the close encounters will be close enough to cause a change in orientation of the central object and that others will lead to a capture of one nucleus by the other. This second situation will lead fairly rapidly to a spiralling close orbit of the two massive compact objects, in which precession will naturally result. This has been discussed, by, e.g., Begelman, Blandford, and Rees (1980) and Whitmire and Matese (1981). A further consequence of a rapid spiral is that the precession angle will increase in time comparable with the precession period. We should also note that even if precession does not occur, orbital velocities comparable with the jet ejection velocities (and these may be up to several tenths of the velocity of light) will cause the jet resultant velocity to swing around in the sky in a way indistinguishable from a precession. Furthermore, the velocity, and hence the cone angle, will increase as the spiralling progresses.

The existence of spiralling jets in the sky around nearby QSOs therefore seems to be a plausible consequence of the idea that they are connected with galaxies disturbed by close encounters—an idea supported by other lines of evidence. In the case of radio galaxies the optical evidence also favors this mechanism. We may speculate a little further: in a precessing binary of supermassive compact objects, accretion on to the active (more massive?) body may well be modulated periodically by its precession and may even lead to enhanced ejection on alternate sides of the object. Even without precession, this may occur if the orbit and spin axes are very differently aligned, which would be the general case coming from a random encounter. Thus we should expect unevenness in the jet intensity which may be periodic of shorter period than the jet precession. We also note the several cases which appear to suggest ejection in alternating opposite directions (Rudnick 1982).

It is of interest to explore the consequences of the deduced precession periods. In the few analogous stellar cases known (Her X-1, LMC X-4, SS 433), the disk precession period lies between 13 and 21 times the binary orbital period. As a rough estimate let us assume that binary periods are 10 times lower than the precession periods given in Table 1. In the case of the QSOs, this gives an average period of about 2000 yr. To estimate masses of the central objects we need to know the orbital velocity, K. Observations of QSOs in groups of galaxies (Stockton 1978) show that QSO velocities are close to those of nearby galaxies, so that $K = 1000$ km s^{-1} may be a reasonable upper limit. With the period of 2000 yr and a mean line-of-sight inclination of 30°, we find that an orbital velocity of 1000 km s^{-1} corresponds to two bodies of mass $2 \times 10^9\ M_\odot$. If one object (the active one?) is 4 times more massive than the other, the masses become 1.5 and $6 \times 10^{10}\ M_\odot$. If, however, the orbital velocity is only 100 km s^{-1}, the masses are 10^3 times lower. (Naturally the real test is to observe velocities of the companions—if any—to the precessing-jet QSOs.) It is worth noting that the masses above are within the range of values considered reasonable for central objects in QSOs. If the periods and velocities deduced are the orbital values themselves, however, masses become very much higher ($\sim 10^{17}\ M_\odot$), and this possibility can be eliminated.

In the low β, longer period galaxies, orbital velocity of 100 km s^{-1} and period 10^5 yr yields equal mass binary objects of $\sim 10^8\ M_\odot$, or 7×10^8 and $3 \times 10^9\ M_\odot$ for a 4 to 1 mass ratio.

In summary, then, we propose that precessing jets are a significant and recognizable phenomenon associated with quasars and interacting galaxies. Improved data on a number of these should allow critical tests of the models and a statistically significant assessment of the frequency of occurrence, duration, and energetics of the phenomenon.

We wish to thank John Baldwin, Ray Carlberg, Ron Ekers, Ed Fomalont, Rick Perley, and Tony Readhead for discussions and data. We would also like to thank David Duncan for his careful work on the diagrams and Mary Ann Potts for coding the early version of the program. A. C. G. gratefully acknowledges support of a NASA grant administered by the AAS.

REFERENCES

Begelmann, M. C., Blandford, R. D., and Rees, M. 1980, *Nature*, **287**, 307.
Blandford, R. D., and Königl, A. 1979, *Ap. J.*, **232**, 34.
Burns, J. O., and Christiansen, W. A. 1980, *Nature*, **287**, 208.
Burns, J. O., Christiansen, W. A., and Hough, D. H. 1981, *Bull. A.A.S.*, **13**, 530.
Crampton, D., and Hutchings, J. B. 1981, *Ap. J.*, **251**, 604.
Ekers, R., Fanti, R., Lari, C., and Parma, P. 1978, *Nature*, **276**, 589.
Fomalont, E. B. 1981, in *IAU Symposium 94, Origin of Cosmic Rays*, ed. G. Setti, G. Spada, and A. W. Wolfendale (Dordrecht: Reidel), p. 121.
Gower A. C., and Hutchings, J. B. 1982, *Ap. J. (Letters)*, **253**, L1.
Heckman, T. M., Miley, G. K., Balick, B., van Breugel, W. J. M., and Butcher, M. R. 1982, preprint.
Hjellming, R. M., and Johnston, K. J. *Ap. J. (Letters)*, **246**, L141.
Högbom, J. A. 1979, *Astr. Ap. Suppl.*, **36**, 186.
Hutchings, J. B., Crampton, D., Campbell, B., Gower, A. C., and Morris, S. C. 1982, *Ap. J.*, **262**, in press.
Hutchings, J. B., Crampton, D., Campbell, B., Pritchet, C. 1981, *Ap. J.*, **247**, 743.
Icke, V. 1981, *Ap. J. (Letters)*, **246**, L65.
Linfield, R. 1981, *Ap. J.*, **250**, 464.
Lonsdale, C. J., and Morrison, I. 1980, *Nature*, **288**, 66.
Machalski, 1982, in *IAU Symposium 97, Extragalactic Radio Sources*, ed. D. S. Heeschen and C. M. Wade (Dordrecht: Reidel), in press.
Miley, G. K. 1971, *M.N.R.A.S.* **152**, 477.
Neff, S. G. 1982, in *IAU Symposium 97, Extragalactic Radio Sources*, ed. D. S. Heeschen and C. M. Wade (Dordrecht: Reidel), in press.
Northover, K. J. E. 1976, *M.N.R.A.S.*, **177**, 312.
Penrose, R. 1959, *Proc. Camb. Phil. Soc.*, **55**, 137.
Perley, R. A. 1981, ESA SP-162, p. 80.
Perley, R. A., Fomalont, E. B., and Johnston, K. J. 1980, *A.J.*, **85**, 649.
Readhead, A. C. B., Cohen, M. H., Pearson, T. J., and Wilkinson, P. N. 1978, *Nature*, **276**, 768.
Rudnick, L. 1982, in *IAU Symposium 97, Extragalactic Radio Sources*, ed. D. S. Heeschen and C. M. Wade (Dordrecht: Reidel), in press.
Ryle, M., and Longair, M. S. 1967, *M.N.R.A.S.*, **136**, 123.
Scheuer, P. A. G., and Readhead, A. C. S. 1979, *Nature*, **277**, 182.
Stannard, D. 1982, in *IAU Symposium 97, Extragalactic Radio Sources*, ed. D. S. Heeschen and C. M. Wade (Dordrecht: Reidel), in press.
Stockton, A. 1978, *Ap. J.*, **223**, 747.
_____. 1982, *Ap. J.*, **257**, 33.
Terrell, J. 1959, *Phys. Rev.*, **116**, 1041.
Ulvestad, J., Johnston, K., Perley, R., and Fomalont, E. 1981, *A.J.*, **86**, 1010.
Whitmire, D. P., and Matese, J. 1981, *Nature* **293**, 722.
Wirth, A., Smarr, L., and Gallagher, J. S. 1982, *A.J.*, **87**, 602.
Wyckoff, S., Wehinger, P. A., and Gehren, T. 1981, *Ap. J.*, **247**, 750.
Yee, H. 1981, private communication.

A. C. GOWER: Department of Physics, University of Victoria, Box 1700, Victoria, B.C., V8W 2Y2, Canada

P. C. GREGORY and W. G. UNRUH: Department of Physics, University of British Columbia, Vancouver, B.C., V6T 2A6, Canada

J. B. HUTCHINGS: Dominion Astrophysical Observatory, 5071 West Saanich Road, Victoria, B.C., V8X 4M6, Canada